PCCP

Accepted Manuscript




ROYAL SOCIETY OF CHEMISTRY

www.rsc.org/pccp

Physical Chemistry Chemical Physics
CREATED USING THE RSC LaTeX PCCP ARTICLE TEMPLATE – SEE www.rsc.org/electronicfiles FOR DETAILS
ARTICLE TYPE www. rsc.org/xxxxxx | XXXXXXXX

# Phase stability, chemical bonding and mechanical properties of titanium nitrides: A first-principles study†

**Shuyin Yu,**[a,b,*] **Qingfeng Zeng,**[a,b] **Artem R. Oganov,**[b,c,d] **Gilles Frapper,**[e] **and Litong Zhang**[a]

***Received Xth XXXXXXXXXX 20XX, Accepted Xth XXXXXXXXX 20XX***
***First published on the web Xth XXXXXXXXXX 200X***
**DOI: 10.1039/b000000x**

We have performed first-principles evolutionary searches for stable Ti-N compounds and have found, in addition to the well-known rock-salt TiN, new ground states $Ti_3N_2$, $Ti_4N_3$, $Ti_6N_5$ at atmospheric pressure, and $Ti_2N$ and $TiN_2$ at higher pressures. The latter nitrogen-rich structure contains encapsulated $N_2$ dumbbells with a N-N distance of 1.348 Å at 60 GPa. $TiN_2$ is predicted to be mechanically stable and quenchable. Our calculations of the mechanical properties (bulk modulus, shear modulus, Young's modulus, Poisson's ratio, and hardness) are in excellent agreement with the available experimental data. Further analyses of the electronic density of states, crystal orbital Hamilton population and electron localization function reveal that the hardness is enhanced by strengthening directional covalent bonds and disappearance of Ti-Ti metallic bonding.

## 1 Introduction

The discovery of new ultra-incompressible materials with novel mechanical and electronic properties is of great fundamental interest and practical importance[1]. Titanium nitride and its derivatives are materials which have many remarkable properties, such as chemical stability, thermal stability, oxidative resistance, good adhesion to substrate, high fracture toughness and high hardness, which lend themselves to a wide range of applications. Its high hardness and corrosion resistance have made it particularly useful for increasing the wear resistance of high speed steel cutting tools[2], while its high conductivity and diffusion barrier have led to its use in semiconductor metallization schemes[3]. In addition, titanium nitride and its derivatives also have been used for tool bit coatings, cosmetic faux gold surfaces, thin film resistors, wavelength selective transparent optical films[4], and energy-saving coatings for windows due to its strong infrared reflection.

Numerous works have been done on stoichiometric rock-salt TiN, but also on the under-stoichiometric $TiN_x$ ($0.67 \leq x \leq 1$)[5]. There are numerous reports on the phase stability, elasticity, electronic, chemical bonding properties[6–8] and film growth[9–11] etc., from the early works of Blaha and Schwarz in 1980s[12,13] to the more recently works[14–16]. However, most of their works focus on the stoichiometric rock-salt TiN, and there are few studies of non-stoichiometric titanium nitrides. Many metals have numerous nitrides, and the question of how many titanium nitride phases do really exist is still a mystery. With this in mind, we decided to explore the crystal structures and possible stoichiometries in the Ti-N system by applying modern computational techniques of the recently developed evolutionary algorithm (USPEX).

TiN was first separated by Story-Maskelyne[17] from a meteorite, and it crystallizes in the well-known rock-salt structure. However, the pressure of phase transformation from rock-salt to CsCl-type structure is still controversial[18–20]. The other known compounds are $Ti_2N$ and $Ti_3N_4$. $\varepsilon$-$Ti_2N$[21] (*P4₂/mnm*) is the most stable phase of $Ti_2N$ at normal conditions, while the $\delta$' phase (*I4₁/amd*) can only exist at high temperatures[22]. Ivashchenko et al.[23] predicted phase transformation sequence $\varepsilon$-$Ti_2N$ $\rightarrow$ $Au_2Te$-type $\rightarrow$ $Al_2Cu$-type with transition pressures of 77.5 and 86.7 GPa, respectively. For the metastable $Ti_3N_4$, Kroll et al.[24] proposed that it adopts the $CaTi_2O_4$-type structure at normal conditions. With increasing pressure, it was proposed to transform first into the $Zr_3N_4$-type structure, and then into the cubic $Th_3P_4$-type structure.

Although titanium nitrides have been studied for decades, a detailed theoretical study of their phase equilibria, electronic and mechanical properties would help to reconcile controversies and possibly predict new technologically useful materials. This is exactly the purpose of the present paper. We hope this

[a] *Science and Technology on Thermostructural Composite Materials Laboratory, School of Materials Science and Engineering, Northwestern Polytechnical University, Xi'an, Shaanxi 710072, PR China*
[b] *International Center for Materials Discovery, School of Materials Science and Engineering, Northwestern Polytechnical University, Xi'an, Shaanxi 710072, PR China*
[c] *Department of Geosciences, Center for Materials by Design, and Institute for Advanced Computational Science, State University of New York, Stony Brook, NY 11794-2100, USA*
[d] *Moscow Institute of Physics and Technology, Dolgoprudny, Moscow Region 141700, Russia*
[e] *IC2MP UMR 7285, Université de Poitiers - CNRS, 4, rue Michel Brunet - TSA 51106 - 86073 Poitiers Cedex 9, France*
[*] *The author to whom the correspondence should be addressed to: Shuyin Yu, Email: yushuyin2014@gmail.com*

study will provide guidance for experimental groups aiming to synthesize those novel crystal structures.

## 2 Computational Methodology

To find all potential $Ti_xN_y$ structures in the binary Ti-N phase diagram, we performed an extensive computational search for stable compounds by using the evolutionary algorithm approach as implemented in the USPEX code[25–27] in its variable-composition mode[28], interfaced with the VASP density-functional package[29]. Evolutionary predictions were performed at pressures 0, 20 and 60 GPa and the number of atoms was allowed up to 24 atoms in a primitive cell. The first generation of structures was produced randomly, and the subsequent generations were obtained by applying heredity (50%), atom transmutation (20%), lattice mutation (15%) operators, while some were produced randomly (15%). These are typical parameters for USPEX calculations, with which efficiency is known to be very high. The details of the search algorithm and its first several applications have been described elsewhere[30].

The first-principles electronic structure calculations were carried out within the framework of density functional theory (DFT)[31,32] within the generalized gradient approximation (GGA) in the Perdew-Burke-Ernzerhof (PBE) form[33]. The interactions between the ions and the electrons are described by the projector-augmented wave (PAW) method[34] with a cutoff energy of 600 eV. The exchange-correlation functional based on the local density approximation (LDA)[35] was also considered in our present work for comparison. Brillouin zone was sampled by uniform Γ-centered Monkhorst-Pack meshes[36] with the resolution $2\pi\times0.03$ Å$^{-1}$, which ensures the error bars of total energies are less than 1 meV/atom. Besides, all forces on atoms were converged to less than 1 meV/Å and the total stress tensor was hydrostatic to the order of 0.01 GPa.

Here we have chosen not to use any special approaches for strongly correlated electrons. One approach, hybrid functionals, is applicable only to insulators - i.e. is not suitable for variable-composition systems and chemical reactions involving metals (e.g. metallic Ti). Another popular approach, DFT+U, requires parameter U, which depends on the valence state - which can be critical for variable-composition calculations involving multiple-valence atoms (such as titanium). At the same time, electron correlations are much less important for early 3*d*-metals (such as Sc, Ti) than for late 3*d*-metals (such as Fe, Co, Ni). Our choice of standard DFT is validated by the fact that our search at atmospheric pressure has found all known stable compounds and their crystal structures. With increasing pressure electron correlations decrease and DFT (LDA, GGA) becomes even more reliable.

Theoretical phonon spectra were calculated based on the supercell method using the PHONOPY package[37] in order to probe the dynamic stability of the predicted $Ti_xN_y$ compounds at different pressures. The elastic constants were calculated from the stress-strain relations, and Voigt-Reuss-Hill (VRH) approximation[38–40] was employed to obtain the bulk modulus $B$, shear modulus $G$, Young's modulus $E$, and Poisson's ratio $\nu$. The theoretical Vickers hardness $H_v$ was estimated by using the Chen's model[41] both at GGA and LDA levels, according to the expression:

$$H_v = 2(\kappa^2 G)^{0.585} - 3 \quad (1)$$

where $\kappa$ is the Pugh ratio: $\kappa$=$G/B$. The directional dependence of the Young's modulus for crystals of different symmetries encountered in this study is given in Supplementary Materials (Supp.).

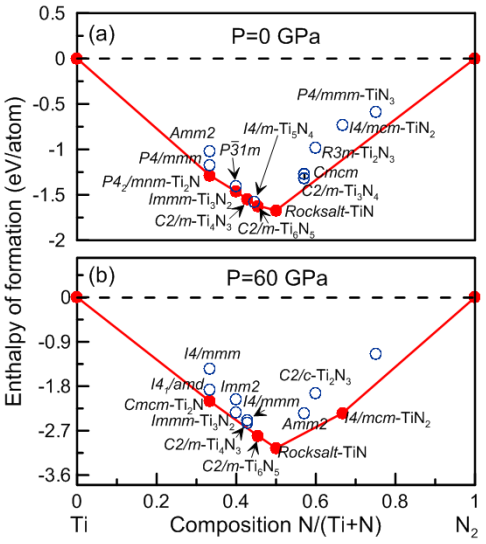


**Fig. 1** (Color online). Convex hull diagrams for Ti-N system at 0 (a) and at 60 GPa (b). Circles denote stable (solid circles) and metastable (open circles) structures. The hexagonal $\omega$-Ti[43] and $\alpha$-$N_2$[44] are adopted as reference states.

## 3 Results and Discussion

Thermodynamics of titanium nitrides can be quantified by constructing the thermodynamic convex hull, which is a complete set of phases stable against transformation into any other phases and decomposition into any set of other phases. These thermodynamically stable phases can be synthesized in principle[42]. The convex hull curves were reconstructed after phonon calculations for the selected thermodynamically stable phases, which are shown in Fig. 1 and Supp. Fig. 6s. Noticeably, our evolutionary simulations succeed in finding the well-known rock-salt TiN and $\varepsilon$-$Ti_2N$ observed by experiments at ambient conditions. In addition, we uncovered three new stable

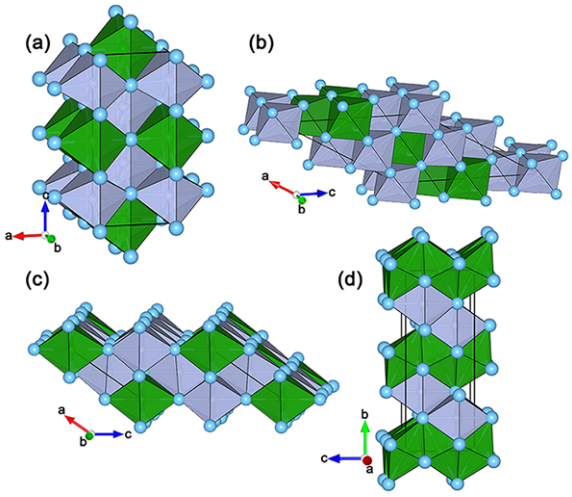


**Fig. 2** (Color online). Crystal structures of Ti-N compounds. (a) *Immm*-$Ti_3N_2$ at 0 GPa, (b) *C2/m*-$Ti_4N_3$ at 0 GPa, (c) *C2/m*-$Ti_6N_5$ at 0 GPa, (d) *Cmcm*-$Ti_2N$ at 60 GPa. The Ti and N atoms are represented as big blue and small gray spheres, respectively, nitrogen vacancies are shown in the green octahedra.

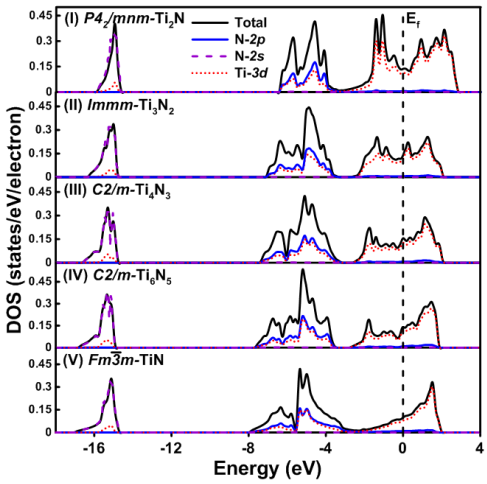


**Fig. 3** (Color online). The total and partial density of states (DOS) for the $Ti_{n+1}N_n$ subnitrides and TiN at zero pressure. Vertical dashed line is the Fermi energy.

compounds, the orthorhombic $Ti_3N_2$, and monoclinic $Ti_4N_3$ and $Ti_6N_5$. At 20 GPa, only the *Immm*-$Ti_3N_2$ phase loses its thermodynamic stability, i.e., becomes a metastable phase. At a higher pressure of 60 GPa, $\varepsilon$-$Ti_2N$ transforms into the orthorhombic *Cmcm* phase, and a new stable nitrogen-rich compound $TiN_2$ is discovered.

The detailed crystallographic data and enthalpies of formation are listed in Supp. Tab. 1s. Note that the enthalpies of formation without the zero point energy (ZPE) correction are only ~0.07 eV/atom different from the ZPE-corrected energies, and convex hulls are not sensitive to ZPE. Thus, for reasons of computational convenience, the zero point energy is omitted for the systematic structural search.

### 3.1 Rocksalt TiN and related subnitrides $Ti_{n+1}N_n$

While TiN has the ideal cubic rocksalt structure, $Ti_3N_2$, $Ti_4N_3$ and $Ti_6N_5$ are versions of this structure with ordered N-vacancies (see Fig. 2) - in $Ti_3N_2$ one third of nitrogen sites are vacant, in $Ti_4N_3$ - one quarter, and in $Ti_6N_5$ - one sixth. Similar vacancy-ordered phases were earlier reported to be stable for hafnium and titanium carbides $M_{n+1}C_n$ (M=Hf and n=2, 5[45]; M=Ti and n=1, 2, 5[46]). Generally, the decrease of vacancy concentration makes the structure denser, less compressible, harder, and more stable under pressure. Indeed, among defective rock-salt phases only $Ti_6N_5$ (with the lowest vacancy concentration) survives as a (barely) stable phase at 60 GPa. $Ti_3N_2$ has space group *Immm*, while $Ti_4N_3$ and $Ti_6N_5$ belong to space group *C2/m*. It is convenient to visualize these structures by N-centered octahedral ($NTi_6$), as shown in Fig. 2. In the $Ti_{n+1}N_n$ series, $Ti_5N_4$ is missing as a stable compound. Nevertheless, a structure with space group *I4/m* is very close to the convex hull, but lies above it (15 meV/atom), i.e., $Ti_5N_4$ is a metastable phase. The convex hull diagram of Ti-N system at finite temperatures is shown in Supp. Fig. 1s. The results yield a conclusion that none of the Ti-N compounds will lose their thermodynamic stability up to 1000 K.

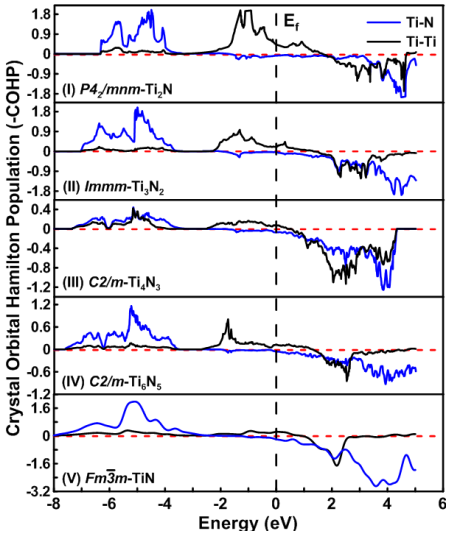


**Fig. 4** (Color online). The calculated crystal orbital Hamilton population (-COHP) for the $Ti_{n+1}N_n$ subnitrides and TiN at zero pressure.

$\varepsilon$-$Ti_2N$ has the anti-rutile structure with space group $P4_2/mnm$. At pressures above 20.8 GPa (Supp. Fig. 3s), tetragonal $\varepsilon$-$Ti_2N$ transforms into an orthorhombic *Cmcm*

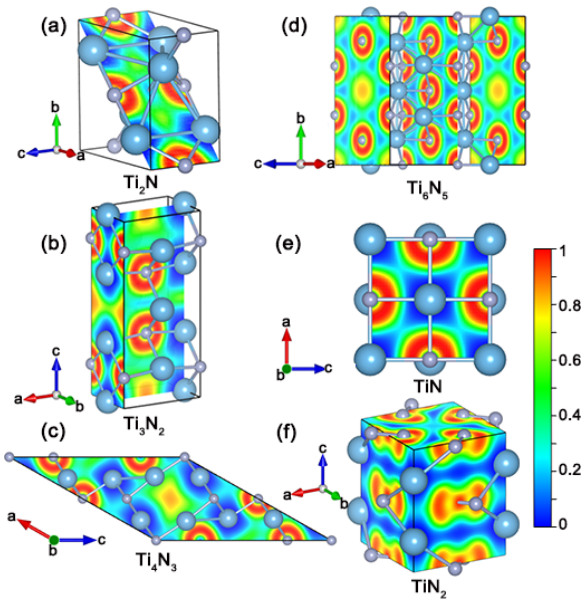


**Fig. 5** (Color online). Calculated electron localization function (ELF) maps for the Ti-N compounds. The blue spheres represent Ti atoms while gray spheres represent N atoms.

structure (see Fig. 2d). This structure contains a distorted close packing of Ti atoms, where one half of octahedral voids are occupied by nitrogen atoms, and edge-sharing $NTi_6$-octahedra form double slabs alternating with nitrogen-free layers. It is noteworthy that the enthalpy of *Cmcm*-$Ti_2N$ is lower by more than 0.24 eV/f.u. than that of the $Au_2Te$-type or $Al_2Cu$-type structures proposed by Ivashchenko et al.[23].

Having investigated the crystal structures and energetics of the various titanium subnitrides $Ti_{n+1}N_n$ and TiN, we now consider their electronic properties. The total and partial densities of states (DOS) of the ground-state compounds are shown in Fig. 3. The crystal orbital Hamilton population (-COHP) curves were calculated by using the LOBSTER package[47] and are displayed in Fig. 4. These orbital-pair interactions can provide a quantitative measure of bond strengths. The positive and negative energy regions in the -COHP curves correspond to bonding and antibonding states, respectively. For $Ti_{n+1}N_n$ structures, the DOS are decomposed into three well separated energy regions: (1) a deeply lowest valence band, $s_N$; (2) a hybridized Ti-*3d*/N-*2p* band, $d_Mp_N$; (3) a partially filled higher lying Ti-*3d* band, $d_M$. The $s_N$ band is dominated by the *2s* orbitals of the nitrogen atoms. Therefore, the contribution of this band to the bonding is not so large. The following upper group of valence bands $d_Mp_N$ is a result of strong hybridization from the *3d* states of Ti atoms and the *2p* states of N atoms. These peaks correspond to the Ti-*3d*/N-*2p* bonding orbitals contribution. Their antibonding counterparts appear well above the Fermi level.

When n goes from 1 to 5 in $Ti_{n+1}N_n$ series, e.g., the number of N-filled $Ti_6$ octahedra increases, the energy region for the Ti-*3d*/N-*2p* peaks is expanded. This energy dispersion is caused by more extensive mixing between Ti-*3d* and N-*2p* orbitals, and suggests the enhancement of the covalency of titanium-nitrogen bonding network. Let us turn our discussion to the upper energy region. From both DOS and COHP analyses, one may see that the bottom of the $d_M$ band is mainly dominated by the bonding orbitals of *3d* Ti atoms and the corresponding DOS exhibits a feature of "near free electron" responsible for metallicity (see Fig. 3). Vacant antibonding Ti-*3d*/N-*2p* and antibonding Ti-*3d*/N-*3d* states compose the bottom of the conduction band. These results confirm the mixed covalent Ti-N and metallic Ti-Ti bonding nature in titanium subnitrides and TiN compounds.

As N content increases, valence band broadens ($d_Mp_N$ band), valence electron concentration increases, and covalent interactions become stronger. This is reflected in shortening of Ti-N bonds: the shortest bond lengths are 2.082, 2.071, 2.069 and 2.022 Å for $Ti_2N$, $Ti_3N_2$, $Ti_4N_3$ and $Ti_6N_5$ at 0 GPa, respectively. In the same sequence the $N(E_F)$ gradually decreases, reaching the lowest value ∼0.098 states/eV/electron for TiN (see Fig. 3). To further explore the bonding nature in each $Ti_{n+1}N_n$ and TiN structures, we examined the electron localization function (ELF)[48] of these Ti-N compounds (see Fig. 5). We find that there are relatively large ELF values between Ti and N atoms, indicating the partially covalent Ti-N interactions. ELF=0.5 can be identified between titanium atoms, suggesting metallic Ti-Ti bonding. All of these results are consistent with the discussion about the DOS and COHP for each structure of $Ti_xN_y$. Also, we can find charge transfer from Ti to N atoms, consistent with Holec et al.[49].

### 3.2 $TiN_2$, a high-pressure structure with $N_2$ dumbbells

At 60 GPa, we uncovered a nitrogen-rich compound $TiN_2$ with the $CuAl_2$-type structure (SG: *I4/mcm*, see Fig. 6a). The formation enthalpy of this *I4/mcm* structure is lower than that of the previously proposed thermodynamic ground state, the $CaC_2$-V-type structure, predicted by Kulkarni et al.[50] at 60 GPa. This new structure is stable against the decomposition into the mixture of TiN and $N_2$ at pressures above 26.6 GPa (Supp. Fig. 4s). To examine the stability of the *I4/mcm* structure, the phonon frequencies were calculated at atmospheric pressure and at 60 GPa, which are shown in Fig. 6b and Supp. Fig. 2s. Imaginary phonon frequencies were not observed in the entire Brillouin zone, indicating that the predicted *I4/mcm* structure is dynamically stable and, if synthesized, might be quenchable at atmospheric pressure.

The structure of $TiN_2$ contains $TiN_8$ face-sharing tetragonal antiprisms stacked along the *c*-axis. Unlike normal $CuAl_2$-type structures, here we have $N_2$-dumbbells encapsu-

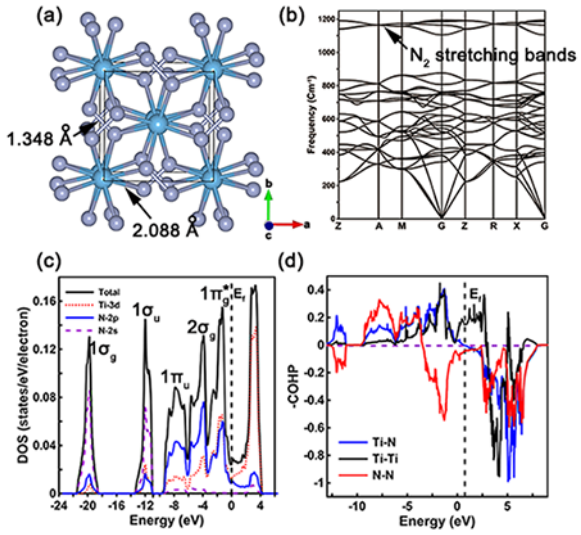


**Fig. 6** (Color online). (a) Crystal structure of *I4/mcm*-$TiN_2$, (b) phonon dispersion curve at 60 GPa, (c) projected and total DOS with symmetry labels of molecular $N_2^{4-}$ filled valence orbitals assigned to each DOS peak at 60 GPa, and (d) -COHP of *I4/mcm*-$TiN_2$ at 60 GPa.

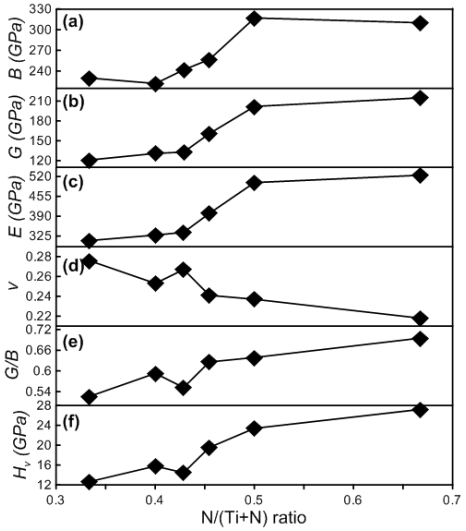


**Fig. 7** (Color online). Calculated bulk modulus $B$, shear modulus $G$, Young's modulus $E$, Poisson's ratio $\nu$, $G/B$ ratio, and Vickers hardness $H_v$ of the titanium nitrides as a function of N content.

lated in cubic $Ti_8$ hexahedra. This topology is identical to the recently predicted stable high-pressure magnesium oxide $MgO_2$[51]. The N-N bond length is calculated as 1.348 Å and 1.378 Å at 60 GPa and 1 atm, respectively. Projected N-2*p* DOS shows that antibonding $1\pi_g^*$ levels are almost fully occupied at 60 GPa (see Fig. 6c). Consequently, for electron counting purposes, the dinitrogen units should be formally considered as $N_2^{4-}$, a pernitride unit isoelectronic to fluorine $F_2$ molecules. Its electronic ground state configuration is $1\sigma_g^2 1\sigma_u^2 1\pi_u^4 2\sigma_g^2 1\pi_g^{*4}$ for 14 valence electrons and its bond order is one (Supp. Fig. 5s). Formally, this leaves the titanium atoms of $TiN_2$ in a $d^0$ configuration ($Ti^{4+}$). Note that a large variety of structures are known with the square antiprismatic geometry and a formally $d^0$ metal center such as $TaF_8^{3-}$ in $Na_3TaF_8$[52].

Stabilizing Ti-Ti interactions in binary Ti-N structures are weakening when nitrogen content increases, e.g., when formal valence $d$ electrons $d^n$ decrease (Ti oxidation number increases). This behavior is structurally reflected by the elongation of the Ti-Ti distances with increasing nitrogen content (shortest Ti-Ti bonds of 2.255 Å and 2.517 Å in $Ti_2N$ and $TiN_2$ at 60 GPa, respectively). Note that the pernitride $N_2^{4-}$ units point directly towards the tetragonal faces of the eight-coordinated titanium atoms (Ti-N bonding length is 2.088 Å at 60 GPa) and are perpendicular to each other in order to minimize the steric clashes between the nitrogen $\sigma$-lone pairs (Pauli repulsions).

### 3.3 Mechanical properties of Ti-N stable structures

The mechanical stability was examined by using the calculated elastic constants (see Tab. 1), and we found that all these phases satisfy the Born-Huang stability criteria[53]. Our calculated elastic constants are in good agreement with the available data[6,54–56]. One can note the large $C_{33}$ values for $Ti_2N$, $Ti_4N_3$, TiN and especially $TiN_2$ (653 GPa from the GGA, 729 GPa from the LDA), which indicate very low compressibility along the $c$-axis. For $TiN_2$, we also find a very large elastic constant $C_{44}$ (336 GPa from the GGA, 364 GPa from the LDA).

The calculated bulk modulus $B$ and shear modulus $G$ are also listed in Tab. 1 and the trend of these mechanical properties as a function of N content for the ground-state structures is shown in Fig. 7. Our calculated results for the well-known rock-salt TiN and $\varepsilon$-$Ti_2N$ are in good agreement with reported values[6,54–56], supporting the accuracy and reliability for other Ti-N compounds. Among these titanium nitrides, TiN has the largest $B$ of 294 GPa from the GGA and 339 GPa from the LDA, which can be comparable to $WB_4$ with a bulk modulus of 328 GPa[57]. A minimum of $B$ appears in $Ti_3N_2$, because this is a vacancy-rich rock-salt phase, and due to the large concentration of vacancies it has unexpectedly low $C_{12}$ and $C_{22}$ values as listed in Tab. 1.

Shear modulus measures the resistance to shape change at constant volume and provides a much better correlation with hardness than bulk modulus[60]. $TiN_2$ has largest shear modulus of 197 GPa from the GGA and 233 GPa from the LDA, which suggests that $TiN_2$ is the hardest material among the

**Table 1** The calculated elastic constants $C_{ij}$, bulk modulus $B$ (GPa), shear modulus $G$ (GPa), Young's modulus $E$ (GPa), Poisson's ratio $\nu$, $\kappa$=$G/B$ ratio, and Vickers hardness $H_v$ (GPa) of the Ti-N compounds at 0 GPa.

| Phase | | $C_{11}$ | $C_{12}$ | $C_{13}$ | $C_{16}$ | $C_{22}$ | $C_{23}$ | $C_{26}$ | $C_{33}$ | $C_{36}$ | $C_{44}$ | $C_{45}$ | $C_{55}$ | $C_{66}$ | $B$ | $G$ | $E$ | $\nu$ | $\kappa$ | $H_v$ |
|---|---|---|---|---|---|---|---|---|---|---|---|---|---|---|---|---|---|---|---|---|
| $Ti_2N$ | GGA | 300 | 214 | 115 | | | | | 442 | | 157 | | | 137 | 214 | 112 | 287 | 0.277 | 0.523 | 11.87 |
| (*P4$_2$/mnm*) | LDA | 353 | 235 | 138 | | | | | 489 | | 184 | | | 147 | 246 | 130 | 332 | 0.275 | 0.528 | 13.38 |
| $Ti_3N_2$ | GGA | 458 | 99 | 125 | | 400 | 115 | | 332 | | 119 | | 145 | 86 | 206 | 124 | 309 | 0.250 | 0.602 | 15.53 |
| (*Immm*) | LDA | 545 | 113 | 140 | | 449 | 140 | | 370 | | 127 | | 172 | 92 | 237 | 138 | 347 | 0.256 | 0.583 | 16.00 |
| $Ti_4N_3$ | GGA | 368 | 150 | 155 | -17 | 393 | 119 | 3 | 421 | -29 | 140 | 10 | 126 | 114 | 225 | 125 | 317 | 0.265 | 0.556 | 14.05 |
| (*C2/m*) | LDA | 412 | 181 | 179 | -16 | 444 | 135 | 8 | 484 | -42 | 167 | 19 | 139 | 130 | 258 | 141 | 357 | 0.269 | 0.547 | 14.84 |
| $Ti_6N_5$ | GGA | 424 | 140 | 145 | -20 | 429 | 146 | 20 | 429 | 1 | 147 | 21 | 158 | 171 | 238 | 151 | 373 | 0.239 | 0.634 | 18.97 |
| (*C2/m*) | LDA | 484 | 161 | 175 | -33 | 490 | 175 | 33 | 481 | 1 | 166 | 34 | 187 | 201 | 275 | 170 | 424 | 0.243 | 0.618 | 20.07 |
| TiN | GGA | 590 | 145 | | | | | | | | 169 | | | | 294 | 189 | 466 | 0.235 | 0.643 | 22.55 |
| (*Fm$\bar{3}$m*) | LDA | 704 | 157 | | | | | | | | 183 | | | | 339 | 215 | 533 | 0.238 | 0.634 | 24.22 |
| | GGA [6] | 583 | 129 | | | | | | | | 179 | | | | 278 | | | | | 24.19 [58] |
| | LDA [6] | 698 | 139 | | | | | | | | 198 | | | | 321 | | | | | |
| | Exp [54] | 625 | 165 | | | | | | | | 163 | | | | 320 | | | | | 23.00 [59] |
| $TiN_2$ | GGA | 535 | 279 | 71 | | | | | 653 | | 336 | | | 148 | 284 | 197 | 481 | 0.218 | 0.693 | 25.64 |
| (*I4/mcm*) | LDA | 631 | 301 | 106 | | | | | 729 | | 364 | | | 185 | 335 | 233 | 567 | 0.218 | 0.696 | 28.75 |

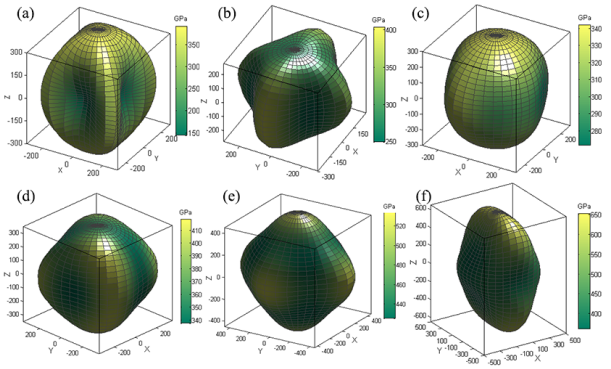


**Fig. 8** (Color online). Directional dependence of Young's moduli (in GPa) for (a) *P4$_2$/mnm*-$Ti_2N$, (b) *Immm*-$Ti_3N_2$, (c) *C2/m*-$Ti_4N_3$, (d) *C2/m*-$Ti_6N_5$, (e) *Fm$\bar{3}$m*-TiN and (f) *I4/mcm*-$TiN_2$.

titanium nitrides. Fig. 7 shows the directional dependence of Young's moduli of the considered Ti-N compounds, and one can clearly see anisotropy from the deviations of its shape from sphere. The Young's modulus along the $c$-axis direction is higher than that along the other directions for $Ti_2N$, $Ti_4N_3$ and $TiN_2$, which agrees well with our above analysis on elastic constants. The Young's modulus is more isotropic in $Ti_4N_3$ and $Ti_6N_5$, while $Ti_2N$, $Ti_3N_2$ and $TiN_2$ show more anisotropy than other Ti-N compounds. For $Ti_2N$, the anisotropy is mainly because of its high $C_{12}$ and low $C_{11}$. $Ti_3N_2$ has just the opposite situation, the low $C_{12}$ and high $C_{11}$ make Young's modulus large in the axis direction and small in the diagonal direction. For $TiN_2$, it is mainly because of its high $C_{44}$.

Poisson's ratio $\nu$ and $G/B$ ratio [61] are indicative of the degree of directionality of covalent bonding. A typical value of $\nu$ is ~0.2 for strong directional covalent materials and ~0.4 for metals. A low Poisson's ratio results from directional bonds, which increase the shear modulus and limit the motion of dislocations, thereby increasing a material's hardness. From Fig. 7, we find that $\nu$ drops down from $Ti_2N$ to $TiN_2$ with increasing N content, except $Ti_4N_3$, which shows a local maximum. For $Ti_4N_3$, we can find that there is significant Ti-Ti metallic bonding in contrast with other Ti-N compounds (see Fig. 4). The large Ti-Ti metallic bonds impair the covalency of this phase, which lead to a local minimum of hardness (see Fig. 7f).

The Vickers hardness was estimated by Chen's empirical method for the ground-state vacancy-ordered Ti-N compounds and listed in Tab. 1. Among the Ti-N compounds, $TiN_2$ has the largest hardness of 26 GPa from the GGA and 29 GPa from the LDA. Note that this is an orientationally averaged value (anisotropy is not considered in Eq. 1). It is no wonder that increasing nitrogen content changes bonding to more directional, the more N is added, the more Ti-N bonds are formed and the less Ti-Ti bonding remains. Based on the analysis of the electronic properties and chemical bonding in those stable Ti-N compounds, we can conclude that with increasing N content, the enhancement of directional covalent interactions and decline of metallicity lead to the increase of the hardness.

## 4 Conclusions

In summary, we have extensively explored the stable structures and possible stoichiometries in the Ti-N system at 0, 20 and 60 GPa by first-principles evolutionary crystal structure prediction. In addition to the well-known phases $Ti_2N$ and TiN, we have uncovered three new intriguing structures at ambient conditions ($Ti_3N_2$, $Ti_4N_3$ and $Ti_6N_5$). At high pressures, two new phases *Cmcm*-$Ti_2N$ and *I4/mcm*-$TiN_2$ were discov-

ered. All those phases are mechanically and dynamically stable at ambient conditions. The calculated elastic constants $C_{ij}$ are in good agreement with the available reported data. Other mechanical properties including bulk modulus, shear modulus, Young's modulus, and Poisson's ratio have been further computed from $C_{ij}$. Among the studied Ti-N compounds, $TiN_2$ possesses the highest hardness of 26 GPa from the GGA and 29 GPa from the LDA. We found a strong correlation between the mechanical properties and N content for the ground-state structures, i.e., the more N content, the more directional covalent Ti-N bonding and the less Ti-Ti metallic bonding, which lead to the enhancement of the hardness. The materials discovered here are attractive for technological applications because of a compromise between hardness and ductility, due to a peculiar interplay between metallicity and covalency.

## 5 Acknowledgement

We thank the Natural Science Foundation of China (Grants No. 51372203 and No. 51332004), the Basic Research Foundation of NWPU (Grant No. JCY20130114), the Foreign Talents Introduction and Academic Exchange Program (Grant No. B08040), the National Science Foundation (Grants No. EAR-1114313 and No. DMR-1231586), DARPA (Grants No. W31P4Q1310005 and No. W31P4Q1210008), and the Government of the Russian Federation (Grant No. 14.A12.31.0003) for financial support. The authors also acknowledge the High Performance Computing Center of NWPU for the allocation of computing time on their machines.

## References

1 H. O. Pierson, *Handbook of refractory carbides and nitrides: properties, characteristics, processing, and applications*, Noyes Publications, 1996.
2 R. Buhl, H. Pulker and E. Moll, *Thin Solid Films*, 1981, **80**, 265–270.
3 M. Wittmer, B. Studer and H. Melchior, *Journal of Applied Physics*, 1981, **52**, 5722–5726.
4 E. Valkonen, T. Karlsson, B. Karlsson *et al.*, 1983 International Techincal Conference/Europe, 1983, pp. 375–381.
5 M. Stoehr, C.-S. Shin, I. Petrov and J. Greene, *Journal of Applied Physics*, 2011, **110**, 083503.
6 K. Liu, X. Zhou, H. Chen and L. Lu, *Physica B: Condensed Matter*, 2012, **407**, 3617–3621.
7 M. Brik and C. Ma, *Computational Materials Science*, 2012, **51**, 380–388.
8 Y. Yang, H. Lu, C. Yu and J. Chen, *Journal of Alloys and Compounds*, 2009, **485**, 542–547.
9 L. H. Dubois, *Polyhedron*, 1994, **13**, 1329–1336.
10 L. H. Dubois, B. R. Zegarski and G. S. Girolami, *Journal of the Electrochemical Society*, 1992, **139**, 3603–3609.
11 A. Sherman, *Journal of the Electrochemical Society*, 1990, **137**, 1892–1897.
12 P. Blaha and K. Schwarz, *International Journal of Quantum Chemistry*, 1983, **23**, 1535–1552.
13 P. Blaha, J. Redinger and K. Schwarz, *Physical Review B*, 1985, **31**, 2316.
14 T. Marten, E. I. Isaev, B. Alling, L. Hultman and I. A. Abrikosov, *Physical Review B*, 2010, **81**, 212102.
15 P. Mayrhofer, F. Kunc, J. Musil and C. Mitterer, *Thin Solid Films*, 2002, **415**, 151–159.
16 K. Weinert and M. Schneider, *Influence of the grinding process on the process behaviour of cutting tools*, Springer, 1999.
17 F. Bannister, *Mineralogical Magazine*, 1941, **26**, 36–44.
18 J. Zhao, L. Yang, Y. Yu *et al.*, *Chinese Physics Letters*, 2005, **22**, 1199.
19 P. Ojha, M. Aynyas and S. P. Sanyal, *Journal of Physics and Chemistry of Solids*, 2007, **68**, 148–152.
20 R. Chauhan, S. Singh and R. K. Singh, *Central European Journal of Physics*, 2008, **6**, 277–282.
21 B. Holmberg, *Acta Chemica Scandinavica*, 1962, **16**, 13.
22 C. De Novion, J. Landesman *et al.*, *Pure and Applied Chemistry*, 1985, **57**, 1391–402.
23 V. Ivashchenko, P. Turchi, V. Shevchenko and E. Olifan, *Physical Review B*, 2012, **86**, 064109.
24 P. Kroll, *Journal of Physics: Condensed Matter*, 2004, **16**, S1235.
25 A. R. Oganov and C. W. Glass, *The Journal of Chemical Physics*, 2006, **124**, 244704.
26 A. R. Oganov, Y. Ma, A. O. Lyakhov *et al.*, *Reviews in Mineralogy and Geochemistry*, 2010, **71**, 271–298.
27 A. R. Oganov, A. O. Lyakhov and M. Valle, *Accounts of Chemical Research*, 2011, **44**, 227–237.
28 A. R. Oganov, Y. Ma, A. O. Lyakhov, M. Valle and C. Gatti, *Reviews in Mineralogy & Geochemistry*, 2010, **71**, 271–298.
29 G. Kresse and J. Furthmüller, *Physical Review B*, 1996, **54**, 11169.
30 A. R. Oganov, *Modern methods of crystal structure prediction*, John Wiley & Sons, 2011.
31 P. Hohenberg and W. Kohn, *Physical review*, 1964, **136**, B864.
32 W. Kohn and L. J. Sham, *Physical Review*, 1965, **140**, A1133.
33 J. P. Perdew, K. Burke and M. Ernzerhof, *Physical Review Letters*, 1996, **77**, 3865.
34 P. E. Blöchl, *Physical Review B*, 1994, **50**, 17953.
35 D. Ceperley and B. Alder, *Vosko SH, Wilk L, Nusair M*

*(1980) Can J Phys*, 1980, **58**, 1200.
36 H. J. Monkhorst and J. D. Pack, *Physical Review B*, 1976, **13**, 5188–5192.
37 A. Togo, F. Oba and I. Tanaka, *Physical Review B*, 2008, **78**, 134106.
38 R. Hill, *Proceedings of the Physical Society. Section A*, 1952, **65**, 349.
39 W. Voigt, *Teubner, Leipzig*, 1928.
40 A. Reuss and Z. Angnew, *Math Meth*, 1929, **9**, 55.
41 X. Chen, H. Niu, D. Li and Y. Li, *Intermetallics*, 2011, **19**, 1275–1281.
42 G. Ghosh, A. van de Walle and M. Asta, *Acta Materialia*, 2008, **56**, 3202 – 3221.
43 Y. K. Vohra and P. T. Spencer, *Physical Review Letters*, 2001, **86**, 3068.
44 R. Bini, L. Ulivi, J. Kreutz and H. J. Jodl, *The Journal of Chemical Physics*, 2000, **112**, 8522–8529.
45 Q. Zeng, J. Peng, A. R. Oganov, Q. Zhu *et al.*, *Physical Review B*, 2013, **88**, 214107.
46 C. Jiang and W. Jiang, *Physica Status Solidi (B)*, 2014, **251**, 533–536.
47 R. Dronskowski and P. E. Bloechl, *The Journal of Physical Chemistry*, 1993, **97**, 8617–8624.
48 A. D. Becke and K. E. Edgecombe, *The Journal of Chemical Physics*, 1990, **92**, 5397–5403.
49 D. Holec, R. Rachbauer, D. Kiener *et al.*, *Physical Review B*, 2011, **83**, 165122.
50 A. Kulkarni, J. Schön, K. Doll and M. Jansen, *Chemistry, an Asian journal*, 2013, **8**, 743–754.
51 Q. Zhu, A. R. Oganov and A. O. Lyakhov, *Physical Chemistry Chemical Physics*, 2013, **15**, 7696–7700.
52 J. K. Burdett, R. Hoffmann and R. C. Fay, *Inorganic Chemistry*, 1978, **17**, 2553–2568.
53 Z. Wu, E. Zhao, H. Xiang *et al.*, *Physical Review B*, 2007, **76**, 054115.
54 R. Ahuja, O. Eriksson, J. M. Wills and B. Johansson, *Physical Review B*, 1996, **53**, 3072–3079.
55 J. Kim, J. Achenbach, P. Mirkarimi *et al.*, *Journal of Applied Physics*, 1992, **72**, 1805–1811.
56 A. Wang, S. Shang, Y. Du *et al.*, *Computational Materials Science*, 2010, **48**, 705–709.
57 M. Wang, Y. Li, T. Cui *et al.*, *Applied Physics Letters*, 2008, **93**, 101905–101905–3.
58 Z. Jiao, S. Ma, X. Zhang and X. Huang, *Europhysics Letters*, 2013, **101**, 46002.
59 A. Szymanski and J. M. Szymanski, *Elsevier Press, Amsterdam*, 1989.
60 H.-Y. Chung, M. B. Weinberger, J.-M. Yang, S. H. Tolbert and R. B. Kaner, *Applied Physics Letters*, 2008, **92**, 261904–261904.
61 S. Pugh, *Philosophical Magazine*, 1954, **45**, 823–843.